

Analysis of the M -shell spectra emitted by a short-pulse laser-created tantalum plasma

M. Busquet

CEA/DIF/DCSA, Boîte Postale 12, 91680 Bruyères-le-Chatel, France

Z. Jiang, C. Y. Côté, and J. C. Kieffer

INRS-Energie, 1650 Boulevard Lionel-Boulet, Case Postale 1020, Varennes, Province, Canada J3X 1S2

M. Klapisch* and A. Bar-Shalom†

ARTEP Inc., Columbia, Maryland 21405

C. Bauche-Arnoult and A. Bachelier

Laboratoire Aimé Cotton, Bâtiment 505, Campus d'Orsay, 91405 Orsay, France

(Received 9 March 1999; revised manuscript received 29 June 1999)

The spectrum of tantalum emitted by a subpicosecond laser-created plasma, was recorded in the regions of the $3d-5f$, $3d-4f$, and $3d-4p$ transitions. The main difference with a nanosecond laser-created plasma spectrum is a broad understructure appearing under the $3d-5f$ transitions. An interpretation of this feature as a density effect is proposed. The supertransition array model is used for interpreting the spectrum, assuming local thermodynamic equilibrium (LTE) at some effective temperature. An interpretation of the $3d-4f$ spectrum using the more detailed unresolved transition array formalism, which does not assume LTE, is also proposed. Fitted contributions of the different ionic species differ slightly from the LTE-predicted values.

PACS number(s): 52.25.Nr, 52.25.Jm, 32.30.Rj

I. INTRODUCTION

M -shell spectra of tantalum have been widely studied in nanosecond laser-created plasma (ns-LPP), for laser pulse lengths of 1 to 30 ns [1–4]. The observed spectra are composed of a few individual lines, and of many “unresolved transition arrays” UTA’s [5] superimposed on large understructures [6], grouped in separated bunches (see Figs. 2–4). These lines and UTA’s are now well identified and correspond to electronic transitions from $n' \geq 4$ to $n = 3$. Isolated lines are emitted by ions isoelectronic to nickel (28 bound electrons), UTA’s are emitted by ions with a few bound electrons more (Cu-like to Se-like) or less (Co-like to Mn-like). For such highly ionized heavy atoms, each UTA is composed of spin-orbit split subarrays (SOSA’S) [7,8]. Each bunch corresponds mainly to a specific transition: $3d-4p$, $3d-4f$, $3d-n'l$ ($n' = 5, 6$). In ns-LPP spectra, the $3d-4f$ arrays, and in a lesser extent the $3d-4p$ arrays, are superimposed on a very large understructure, which is not seen for $n' \geq 5$. The major difference between ns-LPP spectra and the present ps-LPP spectra is the importance of the $3d-5f$ understructure.

The understructure, which is very large for the $3d-4f$ arrays, has been attributed to dielectronic satellites lines [6] of noticeable total oscillator strength [9] and/or to hundreds of faint lines [10]. The net effect is as if producing red wings attached to each resonant and satellite UTA. Piling up these red wings would successfully reproduce the observed spectra [11]. In order to better understand the mechanism producing these understructures, and possibly derive a heuristic model

for the red wings’ intensities and shapes, we are interested to study M -shell spectra emitted by plasmas in different conditions, namely, mostly different densities.

High densities of the regions emitting K -shell spectra have been demonstrated with subpicosecond laser-produced plasmas ps-LPP [12]. In these experiments, high density is a consequence of reduced hydrodynamical expansion due to the short laser-pulse length, and is enhanced by ponderomotive force confinement at high laser intensity [13]. Such mechanisms will still be active with high Z material, so M -shell spectra emitted from dense regions are expected with ps-LPP, and will not be obscured by x-ray emission from low density regions, as the corona expansion is very small.

Goldstein *et al.* [14] have presented a barium spectrum in the range 6–15 Å (which corresponds to the $3d-4f$ transitions) emitted by a plasma produced by a 650-fs laser, with an intensity up to 10^{17} W/cm². They obtained a very large understructure, with a barely resolved UTA superimposed on it. However, in their experiment, the average ionization largely exceeds the Ni-like ion, thus the understructure has a spectral shape very different from the ones we shall present in this paper. Note that the barium spectra presented by Doron *et al.* [15,16] do not present such a feature.

We take advantage of the large energy ($>0.1J$) of the available short-pulse laser to produce tantalum plasmas and to observe the spectrum for different transitions ($3d-4p$, $3d-4f$, and $3d-5f$). We present in this paper identification of the observed UTA in these conditions, a global analysis through supertransition arrays (STA) [17] modeling and a detailed analysis by UTA’s for the $3d-4f$ range. We shall emphasize the differences with typical ns-LPP spectra.

The experimental setup is described in Sec. II, the identification of the lines in Sec. III, and the theoretical analysis in Sec. IV–VI.

*Mailing address: Naval Research Laboratory, Code 6730, Washington, DC 20375.

†Permanent address: NRCN, P.O. Box 9001, Beer-Sheva, Israel.

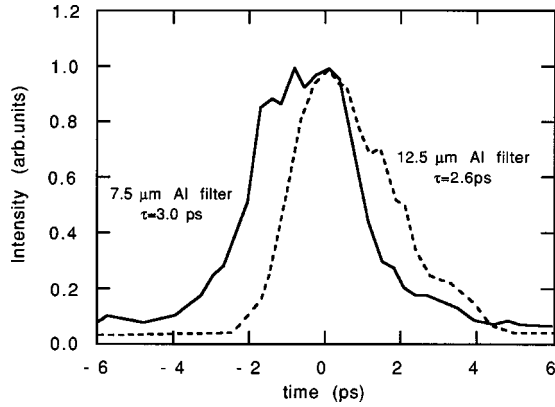


FIG. 1. Time resolved x-ray emission of the Ta target.

II. EXPERIMENTAL SETUP

These experiments were carried out in 1995 with the Table Top Terawatt (T^3) laser system at the Institut National de la Recherche Scientifique (INRS-Québec). A 550-fs, $\lambda = 1.053 \mu\text{m}$ laser pulse with an energy up to 1 J and with a contrast of $10^6:1$ was provided by a Nd:glass system based on the chirped-pulse amplification technique. A potassium dihydrogen phosphate type I crystal was used to double the frequency of the laser light. The resulting pulses had an energy of 450 mJ at a wavelength of $0.527 \mu\text{m}$ with a contrast estimated at better than $10^{10}:1$. This high contrast 400-fs green beam was then focused at normal incidence onto a 100- μm spot by means of a spherical fused silica lens ($f/6$), thus giving an intensity of 10^{16}W/cm^2 .

The x-ray emission (keV range) was studied with various diagnostic including calibrated time-integrated Von-Hámos crystal spectrometer (1–10 keV). *p-i-n* diodes filtered with 55- and 100- μm -thick beryllium filters were used to monitor the x-ray signal and control the beam focussing. Three spectral ranges have been studied (4.2–4.9 Å, 5.3–6.3 Å, and 6.7–7.7 Å). For the first range, the Von-Hámos spectrometer has been internally wavelength calibrated with emission lines (first and second order) from NaCl, V, and Si targets. Wavelength-calibration lines were recorded systematically on each film. The spectral resolution was 5 mÅ at 7 Å. Time-integrated spectra were obtained by accumulation of 10 to 100 shots, depending on the wavelength range considered. The three spectra presented in this paper may then show small differences in temperature from one range to the other, and obviously some averaging in density and temperature conditions takes place. An x-ray streak camera filtered with 7.5 μm and 12.5 μm of aluminum, and having a temporal resolution of 1.6 ps, was used to measure the time history of the keV x-rays. It yielded time duration of the x-ray emissions of less than, respectively, 3.0 and 2.6 ps (see Fig. 1). The duration of the emission was also measured with a pump and probe technique using near-edge x-ray absorption spectroscopy [18]. The inferred duration for Ta emission, assuming a Gaussian temporal shape, at the wavelength of 5 Å (the wavelength of the molecular-absorption resonance), was 1.5 ps full width at half maximum. (FWHM)

III. IDENTIFICATION OF SPECTRAL LINES AND TRANSITION ARRAYS

Three spectral ranges have been studied, 4.2–4.9 Å corresponding principally to the $3d-5f$ arrays, 5.3–6.3 Å cor-

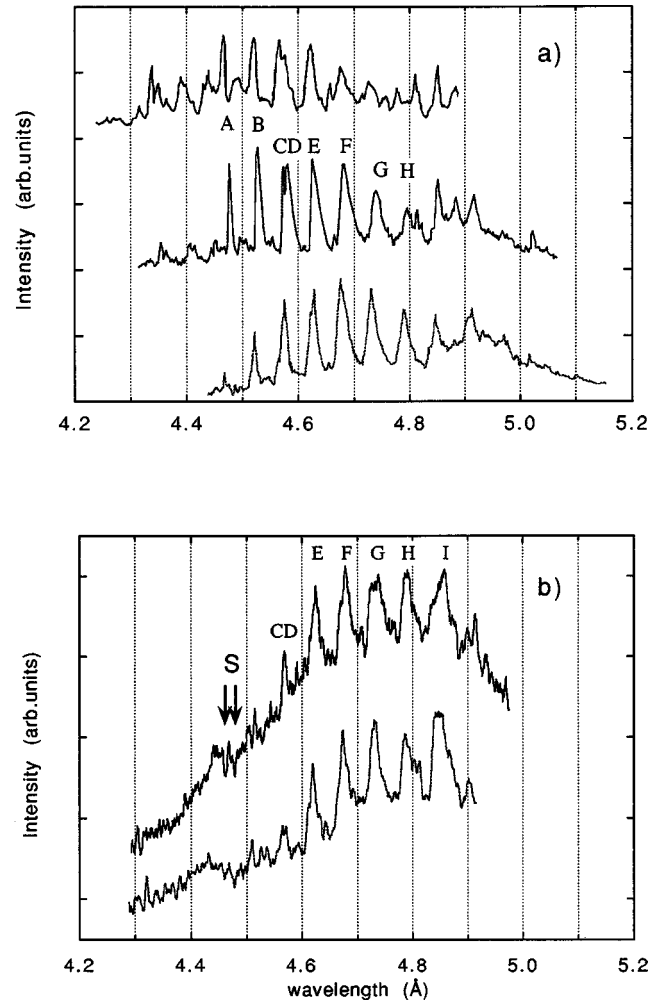


FIG. 2. $3d-5f$ Ta spectrum: (a) with nanosecond pulse-width laser (upper trace: Tragin *et al.* [3], middle trace: Audebert *et al.* [2], lower trace: Bauche-Arnoult *et al.* [6]), (b) with subpicosecond laser (this work, upper trace with a laser intensity $I = 10^{16} \text{W/cm}^2$, lower trace: $I = 5 \times 10^{15} \text{W/cm}^2$). *S* indicates the dips interpreted in the intra-Stark spectroscopy theory [20]. Labels *A–H* stand for Ni-like through Br-like ions, as given in Ref. [2].

responding to the $3p-4d$ and $3d-4f$ arrays, and 6.7–7.7 Å corresponding to the $3d-4p$ arrays (Figs. 2–4).

Initial identification has been obtained by comparison with tantalum spectra recorded from ns-LPP by various team [6,4,2,3]. For the $3d-5f$ arrays, to overcome difficulties in the identification of the lines, wavelengths were calibrated with vanadium (in the second order) and chlorine $K\alpha$ lines. A global comparison of the spectra is shown in Fig. 5. The peaks labeled “Ni” (respectively, “Cu,” “Zn,” “Co”) are lines or UTA’s emitted by ions of 28 (respectively, 29, 30, 27) bound electrons.

We summarize in Table I the transitions and wavelengths of the main Ni-like lines, and corresponding transition probabilities. The computations are performed with the RELAC program [19]. Note that the radiative lifetimes of these transitions are two orders of magnitude shorter than the x-ray emission time. The radiative lifetimes for the other ions are of the same order of magnitude, since they correspond to the same transitions $3d^{10}-3d^9nl$ with some spectator electrons added. The richness of the spectra clearly shows near local

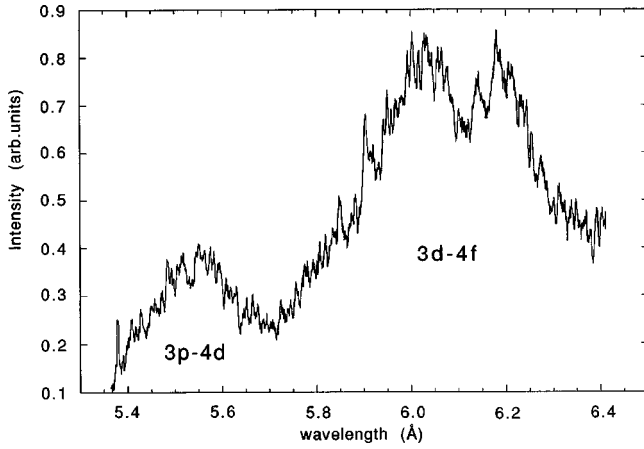


FIG. 3. $3d-4f$ Ta spectrum obtained at INRS (present work). 100 shots of 200 mJ have been used.

thermodynamical equilibrium (LTE) populations. Thus we can infer that the collision rates are at least of the same order of magnitude as the radiative rates. Consequently, the time scale for all atomic processes is much smaller than the duration of the plasma, and it is legitimate to interpret the spectra in the quasi-steady-state approximation. The rms deviation between experimental and calculated wavelengths is 2 mÅ. The $3d^94f$ transition at 5.907 Å, with a deviation of 9 mÅ is an exception, because the upper level would be better characterized in *LS* coupling as $1P1$, for which the exchange term is large enough to distort the wave functions. The same accuracy is to be expected for the other ions, because the supertransition Array (STA) model uses the same parametric potential model as the RELAC. The $3d-4f$ and $3d-5f$ series are clearly separated into two sets by spin-orbit splitting, although there is some overlap between ionization stages.

In the $3p-4d$ range (Fig. 4), Co-like satellites already interpreted by Mandelbaum *et al.* [1] are identified (peaks labeled *A* to *G*, etc., which correspond to Mandelbaum's key). They are superimposed on $M\alpha$ and $M\beta$ inner shell transitions (shaded areas) which start at, respectively, at 7.252 and 7.023 Å.

The blue wing of the $3d-4f$ structure around 5.8 Å (Fig. 5) could be due to Co-like satellites, or even to satellites from higher charge states, but Co-like resonant lines are not visible and even Ni-like lines are not very intense, so time or space averages of emission from hotter plasma (as in Ref. [14]) cannot occur. Such spectral shapes were not seen in ns-LPP spectra.

Identification of the arrays in the $3d-5f$ structure (Fig. 2)

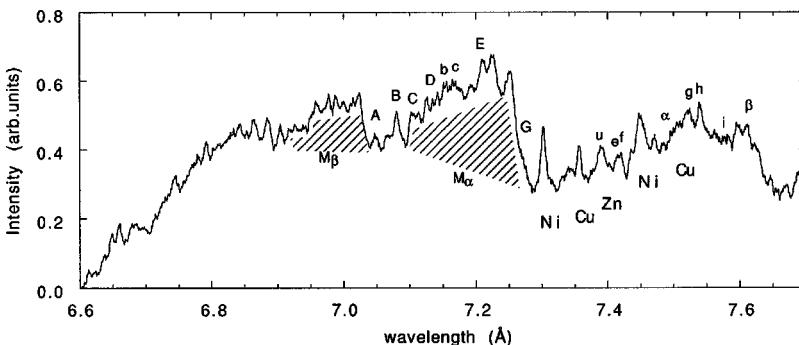


FIG. 4. $3d-4p$ Ta spectrum. The shaded area may be due to inner-shell transitions ($M\alpha$ and $M\beta$). The keys (*A*–*G*, *a*–*u*, α , β) correspond to the identification by Mandelbaum *et al.* [1].

TABLE I. Wavelengths and transition probabilities of the principal Ni-like tantalum (Ta^{45+}) lines. The third and fourth columns are calculated values of the present work.

Transition	λ (Å) (expt.)	λ (Å) (calc.)	A (s^{-1})
$3d^{10}-3d^9_{3/2}4p_{1/2}$	7.447 ^a	7.449	5.67×10^{12}
$3d^{10}-3d^9_{5/2}4p_{3/2}$	7.301 ^a	7.303	1.06×10^{13}
$3d^{10}-3d^9_{5/2}4f_{7/2}$	6.092 ^b	6.089	1.06×10^{14}
$3d^{10}-3d^9_{3/2}4f_{5/2}$	5.907 ^b	5.898	3.63×10^{14}
$3d^{10}-3d^9_{5/2}5f_{7/2}$	4.574 ^c	4.574	9.37×10^{13}
$3d^{10}-3d^9_{3/2}5f_{5/2}$	4.478 ^c	4.477	1.29×10^{14}

^aReference [1].

^bReference [6].

^cReference [2].

by the spectral shape alone would have been ambiguous and may be shifted by one or two arrays, without careful examination. This is why we use wavelength calibration as mentioned earlier. The satellite dips [labeled *S* on Fig. 2(b)] around the line at 4.48 Å are also an indication of an individual resonance line (thus emitted by Ni-like ions) [20]. Frequently observed in *K*-shell resonance lines from ns-LPP, such dips are also observed on the $3p-4d$ spectrum we have obtained in our experiment. Note that, if intra-Stark spectroscopy theory [20] applies to our conditions, an electron density of 10^{22} cm^{-3} would be inferred from the dips separation. The theoretical spectra we shall present in the following are also in accordance with this value. In the $3d-5f$ series, the Ni-like lines are hardly seen, in contrast with other spectral ranges. As the three spectral ranges have been obtained from different series of shots, the respective plasma conditions may slightly differ. Excitation energies are about 2.7 keV for $3d-5f$ arrays, while they are around 2.1 keV for $3d-4f$ and 1.7 keV for $3d-4p$. Consequently, if we assume a temperature of approximately 300 eV (as estimated below), the $3d-5f$ line intensities are expected to be ten times weaker than the $3d-4f$ lines, not accounting for optical depth.

IV. POPULATION MECHANISM OF THE UPPER LEVELS OF THE $3d-4f$ AND $3d-5f$ ARRAYS

The spectrum observed in each of the three spectral ranges corresponds to a given transition (for example $3d-4f$ in the range 5.3–6.3 Å) emitted by various configurations of various ions. Ni-like ion Ta^{45+} emits three isolated lines (the third one being negligible), but all other ions emit unresolved arrays of lines—actually spin orbit split arrays (SOSA's) [7],

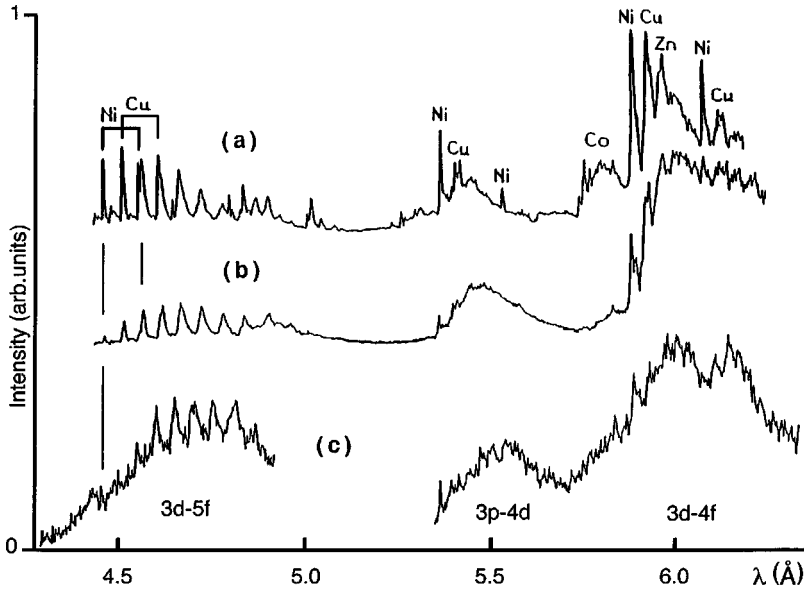


FIG. 5. Ta spectra obtained at LULI [6] for a laser pulse-width of 0.6 ns and a laser intensity of (a) $3 \times 10^{14} \text{ W cm}^{-2}$ and (b) $3 \times 10^{13} \text{ W cm}^{-2}$, compared to (c) spectra obtained at INRS with 0.3 ps, $10^{16} \text{ W cm}^{-2}$ pulses.

three per ion, the third one being also negligible. These in turn coalesce into broad peaks. The peaks, and the underlying broad structure, correspond to hundreds of SOSA's for the given transition (e.g., $3d_{3/2}-4f_{5/2}$ and $3d_{5/2}-4f_{7/2}$) with one or more spectator electrons. Although many of them may have very low oscillator strengths, their large number may yield a considerable intensity and produce the observed understructure, provided there is a significant mechanism to populate the upper levels.

Let us denote $UP_{4J'}^{n'}$ the superconfiguration [17] $3d^9(4l)^{n'}4f_{J'}$, of the ion Ta^{q+} with $n' = q - 28$ electrons in the subshells $4l$, $l = s, p, d$ or f , with one electron in the subshell $4f_{J'}$ and one hole in the $3d$ shell. We shall denote $LO^{n'}$ the corresponding superconfiguration $3d^{10}(4l)^{n'}$. Note that the superconfiguration (SC) $LO^{n'}$ can be considered as a ‘‘ground’’ SC. For the $3d-4f$ arrays, suppose that the spectator electrons and the optical electron lie in the same shell $n = 4$, in such a way that the upper levels of the transitions are close to the ionization limit (say within 100 eV). The energy range of the superconfiguration $UP_{4J'}^{n'}$ extends on both sides of the ionization limit and $UP_{4J'}^{n'}$ is only ‘‘partly autoionizing,’’ so the supertransition array $UP_{4J'}^{n'}-LO^{n'}$ is only partly a dielectronic ‘‘superarray.’’

When local thermodynamical equilibrium (LTE) can be assumed, population mechanisms are, by definition, supposed strong enough so that all levels of the superconfiguration $UP_{4J'}^{n'}$ are populated proportionally to the Boltzmann factor. At lower density, when LTE does not hold, the emitting levels are generally populated by direct excitation from ground states. However, as configurations within $UP_{4J'}^{n'}$ are above and close to the ionization limit, they can also be strongly populated by capture and eventually they will decay radiatively. In our plasma conditions ($N_e \geq 10^{22} \text{ cm}^{-3}$, T_e about a few hundreds of eV) this entrance channel will not be quenched by the $\Delta n = 0$ collisional transition rates to other configurations of $UP_{4J'}^{n'}$, as the radiative decay rates are approximately ten times higher.

Thus, the capture to these autoionizing levels is a significant population channel, even at the lower densities of ns-LPP, and the understructure is always large. On the other hand, for the $3d-5f$ dielectronic satellites SOSA's, the upper levels cannot be populated by capture, as they are farther above the ionization limit (by around 600 eV, see Fig. 6), unless a much larger electron density can increase the capture rates. The $3d-5f$ arrays will present a large understructure when density is high enough to open this entrance channel to the ‘‘levels’’ of the $UP_{5J'}^{n'}$ superconfiguration. Such is the case in our experiment. A schematic description of the different regimes is presented in Fig. 7.

V. ANALYSIS WITH THE STA CODE

We present here an LTE analysis of the whole spectrum. Actually, LTE is not assumed to be completely in force, but the concept of an ionization temperature T_Z that we have

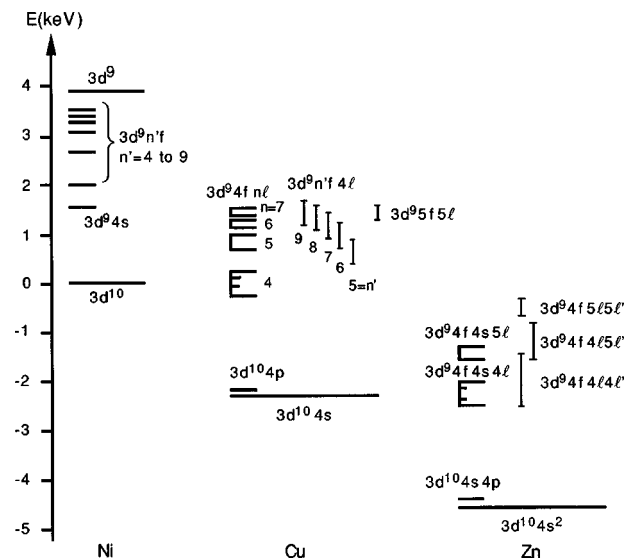


FIG. 6. Energies of some Ta emitting levels (reproduced from Ref. [6]).

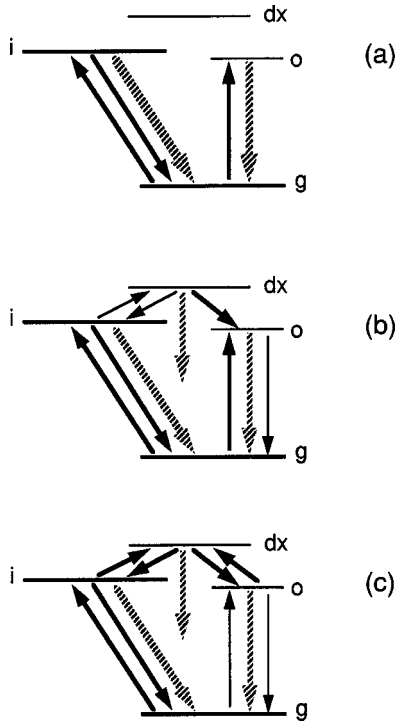


FIG. 7. Schematic population mechanisms, plain and shaded arrows stand for collisional and radiative transitions, respectively. The thickness of the lines indicates approximately the importance of each process: (a) at low density and $n \geq 5$, direct excitation of optical levels *o* from ground levels *g*; (b) high density or $3d-4f$ array: capture from ionized levels *i* to doubly excited *dx*. *dx* levels add an entrance channel; (c) at much higher density, collisional transitions ensure partial LTE among *i*, *dx*, and *o* levels. In this case, radiative transitions do not contribute much to the populations.

introduced and demonstrated recently [21,22] indicates that LTE population distributions at some T_z can reasonably well reproduce the real distribution, specially when not too far from LTE. Describing the population equilibrium among excited levels with an ionization temperature is all the more valid because the density is larger than in ns-LPP, and so is the likely photon reabsorption. The importance of the understructure is also an indication of possible ‘‘partial-LTE’’ conditions, at least at some ionization temperature which may differ from the actual temperature. Furthermore, detailed collisional-radiative calculations performed in the case of germanium have shown that the excited-level populations are close to a ‘‘LTE at T_z ’’ description, when the coupling to the next ionization stage (through capture and autoionization) is large [23], which we have already emphasized.

The relative intensities of the arrays indicate that the most abundant ionic species are Zn-like to Ge-like ions, which means an average charge state $\langle Z \rangle$ in the range of 40–43. An electron density $N_e = 10^{22} \text{ cm}^{-3}$ (which corresponds to a bulk density of $\rho = 0.07\text{--}0.075 \text{ g/cm}^3$) is a good first guess from the expected hydrodynamic conditions of ps-LPP. In LTE conditions, this corresponds to an electronic temperature of $270 \pm 10 \text{ eV}$, computed with a crude hydrogenic model, or $300 \pm 20 \text{ eV}$ computed with the STA model (see Fig. 8). It is noteworthy that the interpretation with the coronal equilibrium model yields a temperature of $900 \pm 100 \text{ eV}$, and an

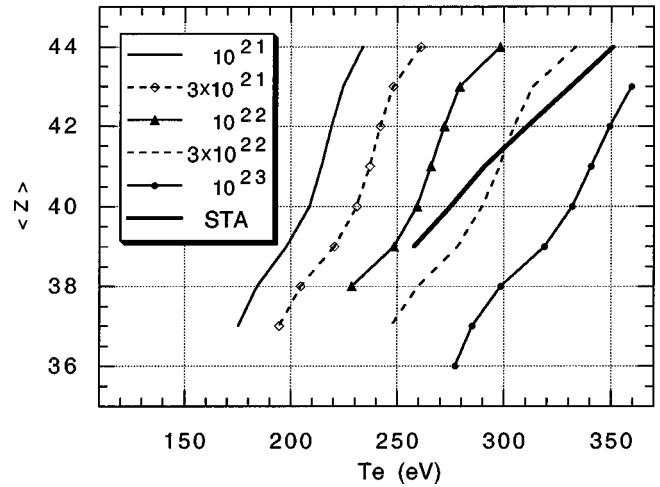


FIG. 8. Ta average charge state $\langle Z \rangle$ computed using a simple hydrogenic LTE model at electronic densities from 10^{21} cm^{-3} to 10^{23} cm^{-3} and using the STA model at $\rho = 0.08 \text{ g/cm}^3$.

optically thin non-LTE model (the mixed model [24]) gives $500 \pm 100 \text{ eV}$. In summary, we can say that 290 eV is a good first guess for the ionization temperature at this assumed density. However, it is well known [25] that in LTE, $\langle Z \rangle$ for a given element is proportional to $T^{3/2}/N_i \exp[-\chi(z)/kT]$ —where $\chi(z)$ is the ionization potential of ion z , and N_i is the ion density. In the present case, the temperature is T_z but the argument is still valid. Therefore, on the basis of $\langle Z \rangle$ only, the temperature could vary from $T_z = 235 \text{ eV}$ for $\rho = 0.008 \text{ g/cm}^3$ to $T_z = 380 \text{ eV}$ for $\rho = 0.8$. This dependence is exemplified in Fig. 8. We will follow the accepted practice of assuming that the density has the value given by the simulation, i.e., $N_e = 10^{22} \text{ cm}^{-3}$. As noted above (Sec. III), this value would also be obtained in the framework of intra-Stark theory [20].

M-shell spectroscopy implies too numerous lines, or even unresolved transition arrays (UTA’s), to allow complete detailed spectrum reconstruction, especially far from coronal equilibrium conditions. Thus, the approach of the supertransition arrays, introduced recently [17] is relevant. The STA approach extends the principle of UTA to superconfigurations, taking advantage of LTE populations through computations of various partition functions. The computations are

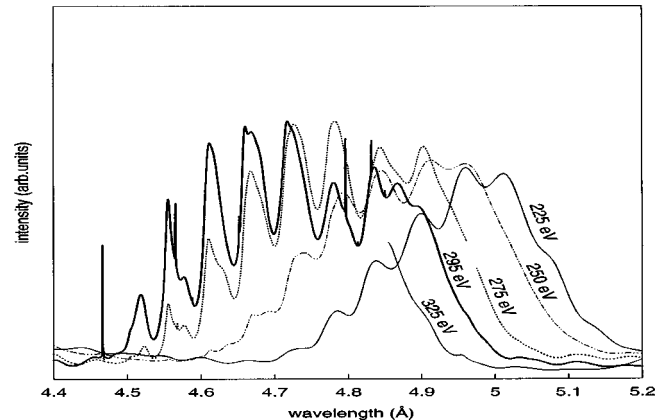


FIG. 9. STA synthetic spectra for $3d-5f$ arrays at $\rho = 0.08 \text{ g/cm}^3$ and different temperatures. Vertical scale varies between curves.

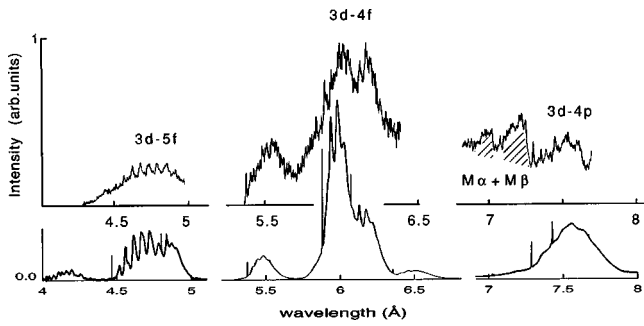


FIG. 10. Experimental spectrum compared with STA synthetic spectrum, for the total observed spectral range at $\rho = 0.08 \text{ g/cm}^3$ and $T_e = 295 \text{ eV}$. The vertical scale is multiplied by 4 and 6 for $3p-4d$ and $3d-5f$ arrays, respectively. The experimental spectrum is shifted upwards for clarity.

done in $j-j$ coupling with a correction for interaction of the relativistic sub-configurations [8], so the supertransition arrays are actually superpositions of SOSA's. In Fig. 9, we plot synthetic spectra at different temperatures for the same bulk density of $\rho = 0.08 \text{ g/cm}^3$. The position of the blue edge of the array is directly related to the effective temperature, and could be considered a diagnostic of the plasma conditions. A good fit of the observed spectrum is obtained for a temperature of $295 \pm 5 \text{ eV}$, not only regarding the position of this blue edge, but also for the global shape and for the intensity ratio of the resonant lines to the understructure.

As seen in Fig. 10, where the $3d-5f$, $3p-4d$, $3d-4f$, and $3d-4p$ arrays are presented, the same conditions ($\rho = 0.08 \text{ g/cm}^3$, $T_e = 295 \text{ eV}$) give good agreement for the shape of the structures of the whole spectrum. In contrast with the study of Goldstein *et al.* [14], we do not need to assume a contribution of x-ray emission from different regions with different temperatures.

VI. REFINED ANALYSIS OF THE $3d-4f$ ARRAYS

In a small range of wave numbers, it is possible to analyze the spectrum in more detail. Indeed, in such plasmas, the emission of seven or eight different ionic species can be observed, and the resulting spectra are very complex. Such a study has already been done for interpreting a ns-LPP spec-

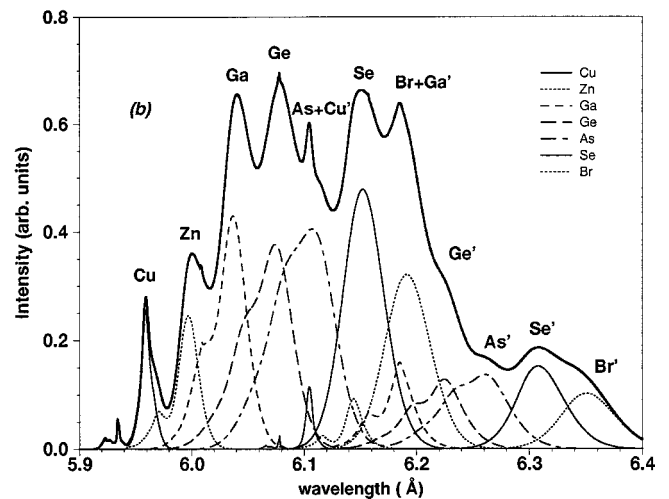
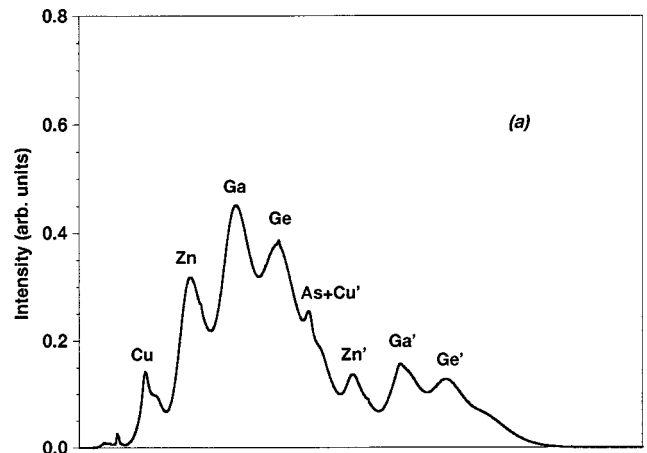


FIG. 11. Synthetic spectra built from 6924 UTA's from seven charge states, (a) $T_e = 300 \text{ eV}$, $N_e = 10^{22} \text{ cm}^{-3}$ and LTE charge distribution, (b) with a fitted distribution, which is wider and leads to an average value of Z lower than the LTE predicted value. The individual contribution of each ion stage is plotted. The transitions $5/2-7/2$ correspond to the primed ion names.

trum (see Ref. [6]). Now, using improved computer codes, thousands of transition arrays can be introduced in the calculation, and the broad understructure under the $3d-4f$ ar-

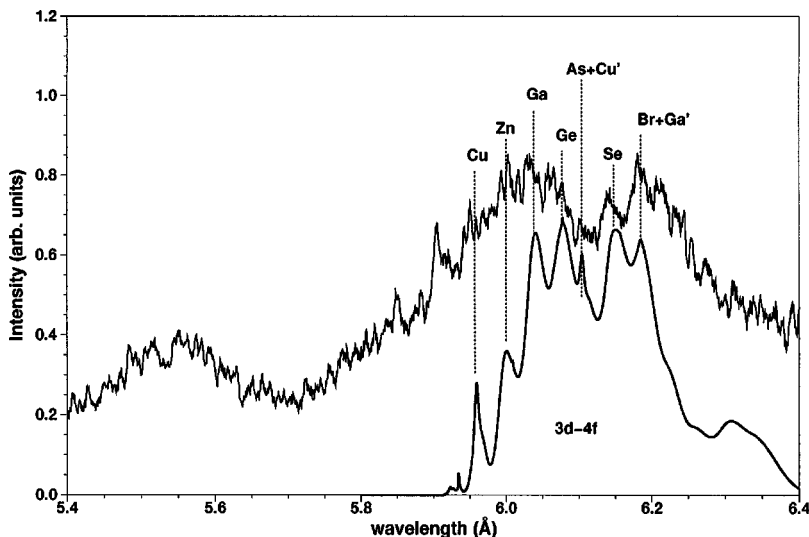


FIG. 12. Comparison of the synthetic spectra of Fig. 11(b) to the experimental spectrum.

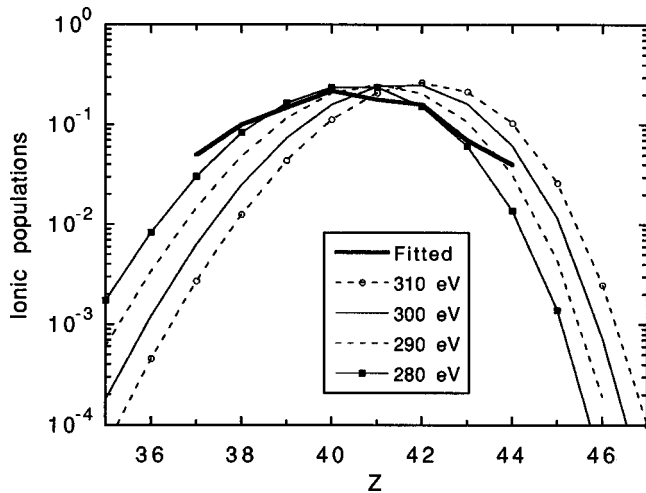


FIG. 13. Comparison of the fitted charge distribution with distributions given by the STA model at different temperatures.

rays can be modeled.

For each ion, we select a set of transitions by the following procedure. The lower configurations are taken among all the configurations having an average energy value (with respect to their respective ground state) lower than a certain limit. We set this limit to 2100 eV, as the Boltzmann factor $\exp(-E/T_Z)$ yields a negligible population ($<10^{-3}$) above this limit. The corresponding upper transitions are deduced by promoting one $3d$ electron to a $4f$ electron.

Each $3d^N-3d^{N-1}4f$ transition array is composed of a few hundreds to a few thousand individual lines. This number grows and becomes huge when 2, 3, or 4 spectator electrons are added. For this reason, we used the unresolved transition array (UTA) formalism [5]. Moreover, in the highly-ionized tantalum spectra, the spin-orbit parameters are large enough for splitting each transition array in two peaks or subarrays (SOSA).

(i) $3d^N(+\text{spect. el.})-3d^{N-1}4f_{5/2}(+\text{spect. el.})$,

(ii) $3d^N(+\text{spect. el.})-3d^{N-1}4f_{7/2}(+\text{spect. el.})$, having the larger wavelength.

Each subarray is represented by a Gaussian profile, whose mean wavelength, FWHM, and total strength are obtained using compact formulas involving Slater and spin-orbit radial integrals [7]. These integrals are computed by means of the RELAC code [19]. Because the interaction between relativistic subconfigurations is taken into account [8], peak (i) (named $3/2-5/2$) is stronger than peak (ii) (named $5/2-7/2$).

Assuming partial LTE between the populations of the upper configurations of each ion, each SOSA is weighted by the Boltzmann factor. We introduce seven charge states, from Cu-like to Br-like ions, to build the spectra shown in Fig. 11. The summation of the two SOSA components results in two broad bands, mostly from 5.9 to 6.1 Å for the

$3/2-5/2$ arrays, and from 6.1 to 6.4 Å for the $5/2-7/2$ arrays. We first started by using an LTE ion distribution at 300 eV [Fig. 11 (a)]. Trying to improve the fit, we varied the temperature. It was found that the experimental ratio of the intensities of these two bands cannot be reproduced by an LTE distribution at any temperature. However, it happens that the average wavelengths of the Se- and Br-like $3/2-5/2$ arrays nearly coincide with the Zn- and Ga-like $5/2-7/2$ arrays [Fig. 1(b)]. Thus, a better agreement is obtained for the gap around 6.15 Å and for the relative intensity of the two bands (see Fig. 12) with a widened and shifted ion distribution (compared to different LTE distributions in Fig. 13). The resulting average $\langle Z \rangle$ is shifted from 41.4 to 40.4, with an rms deviation $\Delta Z=1.75$, instead of 1.5 with STA. The main difference comes for the less abundant ionization stages. Thus, the detailed computations of UTA's allows in this case to detect fine non-LTE effects. It shows that the width of the ion distribution can be a relevant parameter to characterize non-LTE effects, in addition to the average $\langle Z \rangle$.

VII. CONCLUSION

The *M*-shell spectrum of ps-LPP Ta has been recorded and shows a distinctive feature of a large understructure below the $3d-5f$ arrays, in contrast with ns-LPP. Some tentative interpretation is proposed by analysis of the population mechanisms. Not only the $3d-5f$ spectrum, but the whole spectrum including several *M*-shell transitions are successfully reproduced with a fair agreement by an LTE calculation at one temperature ($T=295\pm 5$ eV, for a density of $\rho=0.08$ g/cm³), using the STA code, which includes subconfiguration mixing. This temperature has to be understood as an ionization temperature and the actual electronic temperature is probably larger. A fit to the spectrum has also been obtained by a detailed reconstruction with a large set of SOSA's, and an LTE population distribution at $T_e=300$ eV. However, a better agreement can be obtained by increasing the populations of the less abundant ionic species. This shows that this particular spectrum is very sensitive to departure from Saha ionization distribution. It also shows the interest of measuring the width of the ion distribution, a parameter that has been largely overlooked.

Our modeling was relatively simple, but the agreement with experiment is good. The interpretation of the spectra gives some confidence that we have recorded x-ray spectra from high density plasmas, and shows that ps-LPP are a powerful tool to study dense matter.

ACKNOWLEDGMENT

M.K. and A.B.S. wish to acknowledge the partial support of the U.S. DOE through a contract with the Naval Research Laboratory, Washington, DC.

[1] P. Mandelbaum, M. Klapisch, A. Bar-Shalom, J. L. Schwob, and A. Zigler, Phys. Scr. **27**, 39 (1983).

[2] P. Audebert, J. C. Gauthier, J. P. Geindre, C. Chenais-Popovics, C. Bauche-Arnoult, J. Bauche, M. Klapisch, E. Luc-Koenig, and J. F. Wyart, Phys. Rev. A **32**, 409 (1985).

[3] N. Tragin, J. P. Geindre, P. Monier, J. C. Gauthier, C. Chenais-Popovics, J. F. Wyart, and C. Bauche-Arnoult, Phys. Scr. **37**, 72 (1988).

[4] M. Klapisch, P. Mandelbaum, A. Zigler, C. Bauche-Arnoult, and J. Bauche, Phys. Scr. **34**, 51 (1986); P. Mandelbaum, J. F.

- Seely, A. Bar-Shalom, and M. Klapisch, *Phys. Rev. A* **44**, 5744 (1991).
- [5] J. Bauche, C. Bauche-Arnoult, and M. Klapisch, *Adv. At. Mol. Phys.* **23**, 131 (1987).
- [6] C. Bauche-Arnoult, J. Bauche, E. Luc-Koenig, R. M. More, J. F. Wyart, C. Chenais-Popovics, J. C. Gauthier, J. P. Geindre, and N. Tragin, *Phys. Rev. A* **39**, 1053 (1989).
- [7] C. Bauche-Arnoult, J. Bauche, and M. Klapisch, *Phys. Rev. A* **31**, 2248 (1985).
- [8] J. Bauche, C. Bauche-Arnoult, and M. Klapisch, *J. Phys. B* **24**, 1 (1991).
- [9] J. Bauche, C. Bauche-Arnoult, J. F. Wyart, P. Duffy, and M. Klapisch, *Phys. Rev. A* **44**, 5707 (1991); P. Duffy, M. Klapisch, J. Bauche, C. Bauche-Arnoult, and J. F. Wyart, *ibid.* **44**, 5715 (1991).
- [10] M. Busquet and J. Bruneau, *J. Phys. (France)* **47**, C6-333 (1986).
- [11] M. Busquet, D. Pain, J. Bauche, and E. Luc-Koenig, *Phys. Scr.* **31**, 137 (1985).
- [12] Z. Jiang, J. C. Kieffer, J. P. Matte, M. Chaker, O. Peyrusse, D. Gilles, G. Korn, A. Maksimchuk, S. Coe, and G. Mourou, *Phys. Plasmas* **2**, 1702 (1995).
- [13] O. Peyrusse, M. Busquet, J. C. Kieffer, Z. Jiang, and C. Y. Côté, *Phys. Rev. Lett.* **75**, 3862 (1995).
- [14] W. H. Goldstein, A. Zigler, P. G. Burkhalter, D. J. Nagel, A. Bar-Shalom, J. Oreg, T. S. Luk, A. McPherson, and C. K. Rhodes, *Phys. Rev. E* **47**, 4349 (1993).
- [15] R. Doron, M. Fraenkel, P. Mandelbaum, A. Zigler, and J. L. Schwob, *Phys. Scr.* **58**, 19 (1998).
- [16] R. Doron, E. Behar, M. Fraenkel, P. Mandelbaum, A. Zigler, J. L. Schwob, A. Y. Faenov, and T. A. Pikuz, *Phys. Rev. A* **58**, 1859 (1998).
- [17] A. Bar-Shalom, J. Oreg, W. H. Goldstein, D. Schwarts, and A. Zigler, *Phys. Rev. A* **40**, 3183 (1989).
- [18] F. Raksi, K. Wilson, Z. Jiang, A. Ikhlef, C. Y. Côté, and J. C. Kieffer, *J. Chem. Phys.* **104**, 6066 (1996).
- [19] E. Koenig, *Physica (Amsterdam)* **62**, 393 (1972); M. Klapisch, J.-L. Schwob, B. S. Fraenkel, and J. Oreg, *J. Opt. Soc. Am.* **67**, 148 (1977).
- [20] E. A. Oks, St. Böddeker, and H. J. Kunze, *Phys. Rev. A* **44**, 8338 (1991).
- [21] M. Busquet, *Phys. Fluids B* **5**, 4191 (1993).
- [22] M. Klapisch and A. Bar-Shalom, *J. Quant. Spectrosc. Radiat. Transf.* **58**, 687 (1997).
- [23] M. Busquet and Ph. Cossé, *Spectrosc. Radiat. Transf.* (to be published).
- [24] M. Busquet, *Phys. Rev. A* **25**, 2302 (1982).
- [25] Y. B. Zeldovich and Y. P. Raizer, *Physics of Shock Waves and High-Temperature Hydrodynamic Phenomena* (Academic, New York, 1966), p. 203.